A Massive Spiral Galaxy in the Zone of Avoidance[*]

J. L. Donley[1,2], B. S. Koribalski[1], L. Staveley-Smith[1], R. C. Kraan-Korteweg[3,4],
A. Schröder[5], P. A. Henning[6]

[1] *Australia Telescope National Facility, CSIRO, P.O. Box 76, Epping, NSW 1710, Australia*
[2] *Steward Observatory, University of Arizona, 933 N. Cherry Ave., Tucson, AZ 85721, USA*
[3] *Department of Astronomy, University of Cape Town, Private Bag X3, Rondebosch, 7701, South Africa*
[4] *Depto. de Astronomía, Universidad de Guanajuato, Apdo. Postal 144, Guanajuato, GTO 36000, Mexico*
[5] *Department of Physics and Astronomy, University of Leicester, Leicester LE1 7RH, UK*
[6] *Institute for Astrophysics, University of New Mexico, 800 Yale Blvd., NE, Albuquerque, NM 87131, USA*

ABSTRACT

We report the discovery of a very H I-massive disk galaxy, HIZOA J0836–43, at a velocity of $v_{\rm hel} = 10689$ km s^{-1}, corresponding to a distance of 148 Mpc (assuming $H_0 = 75$ km s^{-1} Mpc^{-1}). It was found during the course of a systematic H I survey of the southern Zone of Avoidance ($|b| \leq 5°$) with the multibeam system at the 64 m Parkes radio telescope. Follow-up observations with the Australia Telescope Compact Array (ATCA) reveal an extended H I disk. We derive an H I mass of 7.5×10^{10} $M_\odot$. Using the H I radius, we estimate a total dynamical mass of 1.4×10^{12} $M_\odot$, similar to the most massive known disk galaxies such as Malin 1. HIZOA J0836–43 lies deep in the Zone of Avoidance ($\ell, b = 262°.48, -1°.64$) where the optical extinction is very high, $A_{\rm B} = 9^{\rm m}.8$. However, in the near-infrared wavebands, where the extinction is considerably lower, HIZOA J0836–43 is clearly detected by both DENIS and 2MASS. Deep AAT near-infrared ($K_{\rm s}$ and H-band) images show that HIZOA J0836–43 is an inclined disk galaxy with a prominent bulge (scale length 2.5″ or 1.7 kpc), and an extended disk (scale length 7″ or 4.7 kpc) which can be traced along the major axis out to a radius of 20″ or 13.4 kpc (at 20 mag arcsec^{-2} in $K_{\rm s}$). The H I disk is much more extended, having a radius of 66 kpc at 1 $M_\odot$ pc^{-2}. Detections in the radio continuum at 1.4 GHz and at 60 μm (IRAS) are consistent with HIZOA J0836–43 forming stars at a rate of $\sim$35 $M_\odot$ yr^{-1}. We compare the properties of HIZOA J0836–43 with those of the most H I-massive galaxies currently known, UGC 4288, UGC 1752 and Malin 1, all of which are classified as giant low surface brightness galaxies.

Key words: galaxies: individual (HIZOA J0836–43) — galaxies: formation

1 INTRODUCTION

Hierarchical models of structure formation in the early Universe predict that massive galaxies begin to form from the merging of low-mass systems at early times and that the mass and luminosity functions for galaxies evolve in a self-similar manner (Press & Schechter 1974; Cole et al. 2000). Such models (Kauffmann, White & Guiderdoni 1993; Klypin et al. 1997) predict large numbers of old low-mass systems and relatively small numbers of young high-mass systems.

However, the detailed match between observations and predictions of the mass function is poor. Two well-documented discrepancies are (1) the small number of low-mass systems observed in the local Universe (Davies, Sabatini & Roberts 2004) and (2) the large number of massive, distant red galaxies, implying a significant density of massive galaxies at early times (Foerster Schreiber et al. 2004).

These discrepancies most probably arise because of the fundamental role of gas physics (supernova and AGN feedback, etc.) in determining the star-formation efficiency in halos of different mass (Kay et al. 2002). Indeed, a recent attempt to incorporate gas physics by the application of a suite of semi-analytic models to the Millennium run (Croton et al. 2006, Springel et al. 2005) has been remarkably suc-
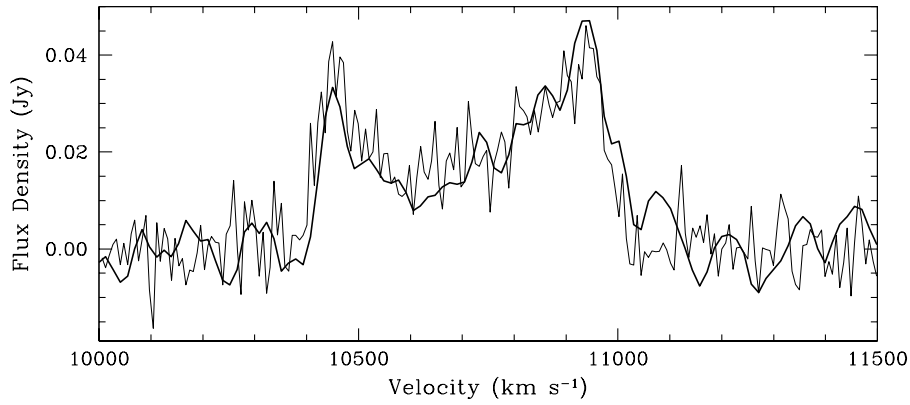
Figure 1. Global H I profile of the galaxy HIZOA J0836–43 as obtained with the 64-m Parkes telescope (thick line) and the ATCA 750D-array (thin line).

cessful in reproducing the exponentially decreasing volume density of objects more luminous than a characteristic value L^*, as well as the observation that massive galaxies tend to contain older stars than low-mass systems.

Due to the sharp decline in the number of galaxies with $L > L^*$ (or $M > M^*$), large samples are needed to constrain the high-luminosity and high-mass ends of the galaxy luminosity and mass functions. In the optical, such a sample is provided by the 2dF Galaxy Redshift Survey, from which Norberg et al. (2002) find $M_{b_j}^* = -19.^{\rm m}0$ ($H_0 = 75 \mathrm{~km\,s^{-1}\,Mpc^{-1}}$) and a slight tendency for an overabundance of massive galaxies relative to a Schechter fit (although they comment that magnitude errors are mostly able to account for this deviation). Similar results are obtained from the Sloan Digital Sky Survey (Blanton et al. 2003).

To sample the high-mass end of the H I mass function, blind H I surveys such as the H I Parkes All-Sky Survey (HIPASS) are required. HIPASS is a systematic H I survey of the southern sky within the radial velocity range of $-1200 < cz < 12700 \mathrm{~km\,s^{-1}}$ (Meyer et al. 2004). Zwaan et al. (2005) find a characteristic mass in neutral hydrogen gas of $M_{\rm HI}^* = 6.3 \times 10^9 ~M_\odot$ ($H_0 = 75 \mathrm{~km\,s^{-1}\,Mpc^{-1}}$), using a catalogue of 4315 H I galaxies from HIPASS. The mass function remains ill-constrained at the high-mass end, however, due to the increasing sparsity of high H I-massive galaxies.

We report here on the discovery and detailed properties of the most massive galaxy in the H I Zone of Avoidance Survey (HIZOA), a deep Parkes H I multibeam survey in the obscured region along the Galactic Plane (§2) (see Donley et al. 2005, Kraan-Korteweg et al. 2005, and Henning, Kraan-Korteweg, & Staveley-Smith 2005 for preliminary results). This galaxy, HIZOA J0836–43, is also the most H I-massive galaxy in the southern and northern-extension HIPASS catalogues, which consist of 4315 and 1003 H I sources, respectively (Meyer et al. 2004, Wong et al. 2005). At the mass of HIZOA J0836–43, $M_{\rm HI} = 7.5 \times 10^{10} ~M_\odot$, the volume density is $1.4 \times 10^{-9} \mathrm{~Mpc^{-3}~dex^{-1}}$, a factor of 10^6 times smaller than the corresponding value at $M_{\rm HI}^*$.

A study of massive gaseous (and stellar) systems is of considerable interest in assessing whether the details of various galaxy formation scenarios, particularly the processes of merging and star-formation, remain viable under the most extreme conditions. The H I-massive galaxy to have received

most attention is Malin 1, whose H I mass is reported to be somewhere in the range $5-10 \times 10^{10} ~M_\odot$ (Bothun et al. 1987; Pickering et al. 1997; Matthews et al. 2001)[1]. Malin 1's high H I mass but low optical surface brightness is of interest in that it raises the possibility of a cosmologically significant amount of gas being locked up in such systems. However, such a population is not known to exist at the sensitivities of existing H I surveys (Rosenberg & Schneider 2002; Zwaan et al. 2003).

The radio and infrared properties of the newly-discovered galaxy are detailed in §3. In §4, we look at the H I and dynamical mass of HIZOA J0836–43, its star-formation rate, morphology, location on the Tully-Fisher relation, and environment. A comparison with other H I-massive galaxies is given in §5, followed by our conclusions in §6.

2 DISCOVERY OF HIZOA J0836–43 WITH THE PARKES TELESCOPE

The galaxy HIZOA J0836–43 was first detected in the deep H I Zone of Avoidance (ZOA) survey made with the Parkes 64-m telescope between March 1997 and June 2002 (see Kraan-Korteweg et al. 2005). This blind survey utilised the Parkes 21-cm multibeam receiver, an array of 13 beams each with two orthogonal linear polarisations (for a detailed description see Staveley-Smith et al. 1996). The data were calibrated and gridded using the *aips++* programs LIVE-DATA and GRIDZILLA, respectively; after gridding the beam width is 15.′5. The data reduction is nearly identical to that of HIPASS (see Barnes et al. 2001, Henning et al. in preparation). The H I Zone of Avoidance survey covers the Galactic longitude range $52° < \ell < 196°$, comprising the southern Milky Way (Henning et al. in preparation) plus a northern extension (Donley et al. 2005), for the most opaque part of the ZOA, i.e. the latitude range $-5° < b < 5°$. With a correlator bandwidth of 64 MHz divided into 1024 channels and an instantaneous velocity
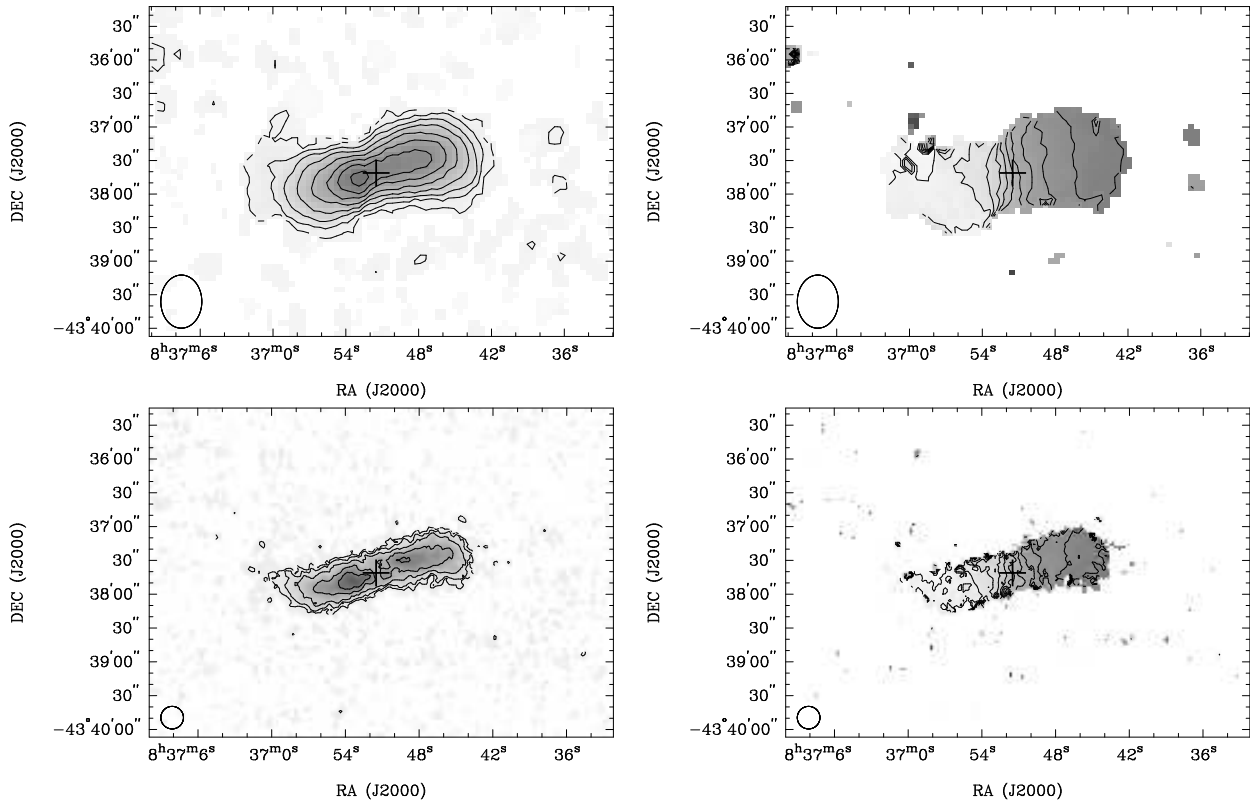
Figure 2. H I distribution (left) and mean H I velocity field (right) of the galaxy HIZOA J0836–43. Contour levels are 0.1, 0.3, 0.6, 1, 1.5, 2.0, 2.5, and 3.0 Jy beam^{-1} km s^{-1} (top left; 1 Jy beam^{-1} km s^{-1} equals an H I column density of 6.8×10^{20} cm^{-2}), 0.1, 0.2, 0.4, 0.8, 1.2, and 1.6 Jy beam^{-1} km s^{-1} (bottom left; 1 Jy beam^{-1} km s^{-1} equals an H I column density of 3.0×10^{21} cm^{-2}), and 10450 to 10950 km s^{-1} in steps of 50 km s^{-1} (right). The synthesized beam is shown in the bottom left corner of each frame ($47.5'' \times 36.7''$ on the top, and $20''$ on the bottom). The cross marks the galaxy centre as determined from the 20-cm radio continuum (see Table 2).

coverage of $-1200 < cz < 12700$ km s^{-1}, the velocity spacing per channel is 13.2 km s^{-1}, or 26 km s^{-1} after Hanning smoothing. The approximate total integration time is 2100 sec beam^{-1}, resulting in an rms of 6 mJy beam^{-1} in large parts of the survey. Results of a shallow subset with an rms of 15 mJy beam^{-1}, the ZOA H I-shallow survey (HIZSS), are given in Henning et al. (2000).

While visually inspecting the data cube centred on $\ell = 264°$, an exceptionally strong signal ($S_{\rm peak} = 47$ mJy beam^{-1}; see Fig. 1) for its very high velocity ($v_{\rm hel} \approx 10700$ km s^{-1}) was initially identified at α, δ(J2000) $= 08^{\rm h}\,36.9^{\rm m}$, $-43° \, 38'$ ($\pm 3'$) or $\ell = 262°.5, b = -1°.6$. The detected H I source, named HIZOA J0836–43, remains unresolved in the Parkes data.

As seen in Fig. 1, the H I signal of HIZOA J0836–43 is exceptionally broad with a velocity width of $\Delta v \approx 600$ km s^{-1}. Using the Parkes data we measure an H I flux density of 13.2 Jy km s^{-1} corresponding to an H I mass of $M_{\rm HI} = 7 \times 10^{10} \, M_\odot$ (assuming $D = 148$ Mpc, see Section 3.1.1). This same signal was later independently identified in the recently released H I catalogue (HICAT, Meyer et al. 2004) obtained from HIPASS. It is listed there as HIPASS J0836–43. The H I parameters extracted from the respective surveys are given in Table 1.

Detailed investigation of HIZOA J0836–43 is extremely difficult due to its location behind the Milky Way. According to the DIRBE/IRAS dust extinction maps of Schlegel et al. (1998) the B-band extinction at the position of HIZOA J0836–43 is $A_{\rm B} = 9^{\rm m}.8$, although we caution that the data in the Galactic plane are not yet well calibrated. Not unexpectedly, this galaxy has no known optical counterpart, and inspection of the DSS images reveal only a very faint R-band counterpart. The corresponding extinction in the near-infrared (NIR) I, J, H, and K bands is much lower: $A_{\rm I} = 4^{\rm m}.4$, $A_{\rm J} = 2^{\rm m}.2$, $A_{\rm H} = 1^{\rm m}.3$, and $A_{\rm K} = 0^{\rm m}.8$, respectively. DENIS (IJK; Epchtein 1997) and 2MASS (JHK; Jarrett et al. 2000) reveal two and three possible counterparts, respectively, in all the wavebands, 2MASX J08365157–4337407, 2MASX J08370723–4339137 and 2MASX J08363600–4337556. As discussed in §3.1.1 and §3.2, the counterpart to HIZOA J0836–43 is 2MASX J08365157–4337407, a galaxy with an inclination of $\sim 66°$.

3 RADIO AND INFRARED RESULTS

3.1 ATCA radio observations

H I line and 20-cm radio continuum observations of the galaxy HIZOA J0836–43 were obtained with the Australia Telescope Compact Array (ATCA) in the 750D and the 1.5D configurations. The observations took place on 2003 February 10 and November 28, respectively, with a total integration time of $\sim 2 \times 12$ hours. For the H I line observations, we used a centre frequency of 1371 MHz and a band-
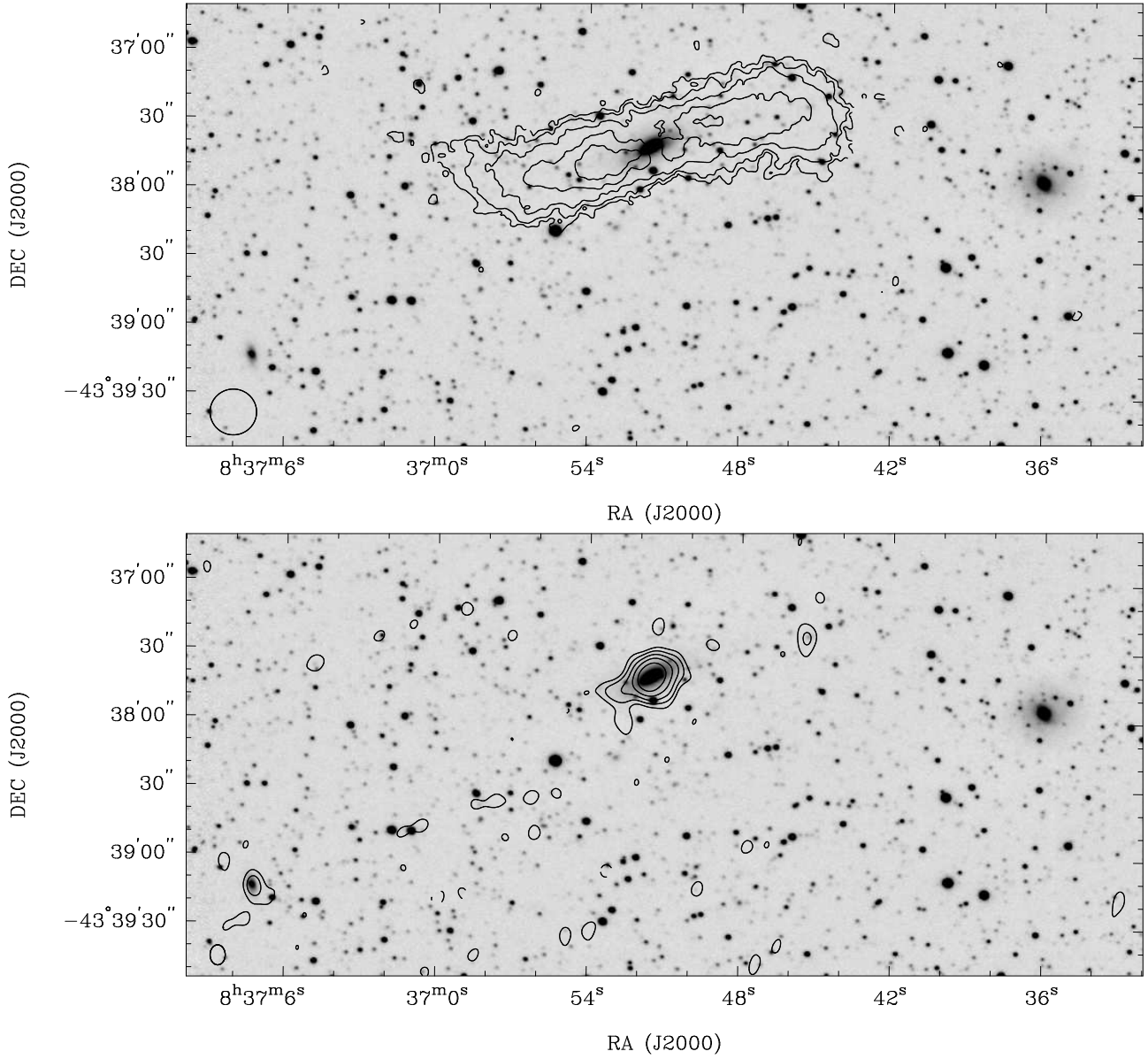
Figure 3. Top: H I distribution of HIZOA J0836–43 (contours) at a resolution of 20″ overlaid onto the AAT $K_{\rm s}$-band image (greyscale). The contour levels are the same as in Fig. 2 (bottom left). **Bottom:** 20-cm radio continuum image of HIZOA J0836–43 (contours) overlaid onto the same K-band image. The contour levels are –0.26, 0.26, 0.52, 1.04, 2.08, and 4.16 mJy beam^{-1}; the synthesized beam is 8.7″ × 6.5″. The displayed region was chosen to also include the two neighbouring galaxies, one of which is detected in the radio continuum with an H I flux density of $\sim$ 1 mJy.

width of 8 MHz, divided into 512 channels. This resulted in a channel width of 3.4 km s^{-1} and a velocity resolution of 4.1 km s^{-1}. The wide-band 20-cm radio continuum observations were centred on 1384 MHz with a bandwidth of 128 MHz, divided into 32 channels. We used PKS B1934–638 as primary calibrator and PKS B0823–500 as secondary calibrator. Their flux densities are 15.0 Jy and 5.5 Jy at 1378 MHz, respectively. Data reduction was carried out with the MIRIAD software package using standard procedures.

Various H I line data cubes were made to investigate the neutral hydrogen distribution and kinematics of the galaxy HIZOA J0836–43. The best results were obtained by using 'natural' weighting of the combined *uv*-data sets. Including all baselines resulted in an angular resolution of

18.9″ × 18.8″; we used a restoring beam of 20″ and a channel width of 10 km s^{-1}. By excluding the longest baselines (i.e. all baselines to antenna 6) we obtain an angular resolution of 47.5″ × 36.7″. We measure an rms per channel of 1.2 mJy beam^{-1} and 1.4 mJy beam^{-1}, respectively. The resulting H I distribution and mean H I velocity field of HIZOA J0836–43 for both angular resolutions are shown in Fig. 2.

Radio continuum images were made using 'robust' (r = 0) and 'uniform' weighting of the combined *uv*-data, resulting in angular resolutions of 10.3″ × 9.0″ and 8.7″ × 6.5″, respectively. The measured rms is $\sim$0.1 mJy beam^{-1}. We find a continuum source at the position of HIZOA J0836–43 that is slightly extended along a position angle of $PA =$
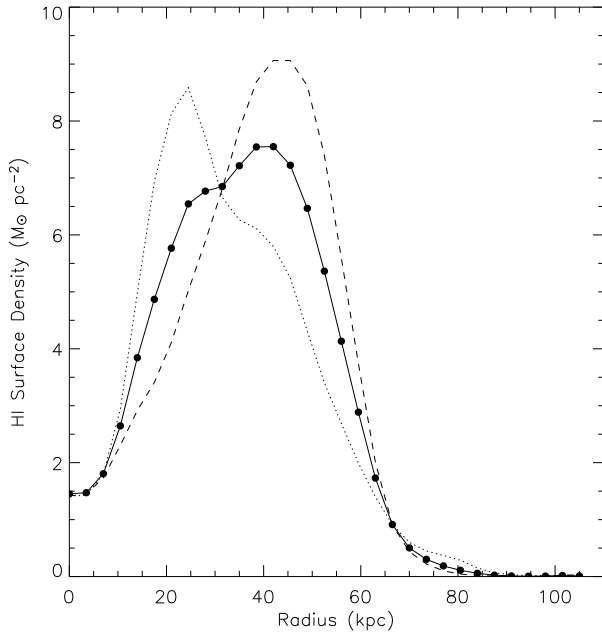
Figure 4. Radial H I density profile of HIZOA J0836–43, obtained with the program RADIAL in the software package GIPSY. The solid line (and filled circles) gives the average profile, whereas dotted and dashed lines give the H I profile of the approaching and receding sides, respectively.

125° and that has an integrated 20-cm flux density of ∼24 mJy.

3.1.1 Global HI properties

The global H I spectra of HIZOA J0836–43 (see Fig. 1) were analysed using the MIRIAD program MBSPECT. Because the galaxy was unresolved in the Parkes H I data, its spectral profile was formed by weighting the flux according to the beam parameters. In the ATCA H I data, HIZOA J0836–43 is clearly resolved and consequently the spectral profile was taken to be the sum of the flux in a conservative box of 3.8×2.2, centred on the galaxy. For both the Parkes and ATCA H I data, first-order baselines were fit to the spectra and the total H I flux density was then determined by integrating over the galaxy profile.

The systemic velocity was taken to be the midpoint of the spectral profile at the 50% H I peak flux level. From a heliocentric velocity of $v_{\mathrm{hel}} = 10689$ km s^{-1} ($z = 0.036$), we calculate a velocity in the Cosmic Microwave Background (CMB) frame of $v_{\mathrm{CMB}} = 10928$ km s^{-1}, where the CMB vector was taken from Fixsen et al. (1996). Adopting a Hubble constant of $H_0 = 75$ km s^{-1} Mpc^{-1} and a cosmology with $\Omega_{\mathrm{m}} = 0.3$ and $\Omega_{\lambda} = 0.7$, we derive a cosmological luminosity distance of $D = 148$ Mpc (see Table 2). At this distance, $1'$ corresponds to 40.1 kpc.

The 20% and 50% velocity widths were measured using a width-maximizing technique. The measured H I properties for both observations are given in Table 1, where they are compared with equivalent measurements from HICAT (Meyer et al. 2004). For the remainder of the paper, we adopt the ATCA velocity widths of $w_{20} = 610 \pm 9$ km s^{-1} and $w_{50} = 566 \pm 6$ km s^{-1}. Uncertainties in the integrated

flux density and velocity measurements were derived using the formulas given in Koribalski et al. (2004).

Fig. 3 shows the K_{s}-band image obtained with the AAT (see §3.2 for further details) overlaid onto the H I distribution (upper panel) and continuum distribution (lower panel) as obtained from the high-resolution ATCA H I data cube. Both the H I and the 20 cm continuum measurements identify the galaxy 2MASX J08365157–4337407 as the counterpart to HIZOA J0836–43. The other two galaxies, 2MASX J08363600–4337556 and 2MASX J08370723–4339137, lie at distances of 2.8 and 3.2 from HIZOA J0836–43, respectively.

3.1.2 HI radial density profile

We measure the H I radial density profile from the H I total intensity map of HIZOA J0836–43, using the iterative method of Lucy (1974) as applied by Warmels (1988) and implemented in the program RADIAL in the software package GIPSY (van der Hulst et al. 1992). Because this method assumes that the H I has a planar and axisymmetric distribution, it is limited in its detection of structures such as spiral arms and warps. However, for highly-inclined galaxies observed with low angular resolution, such as HIZOA J0836–43, this method provides the most accurate means of measuring the surface density distribution. Another advantage of the Lucy method is that the surface density is measured directly; we need not assume a given model to which the data are fit. In addition, the density profile can be measured independently for the two sides of the galaxy.

The H I radial density profile for HIZOA J0836–43 as derived from the low resolution H I distribution (Fig. 2, left) is given in Fig. 4. The density profiles of both the approaching and receding sides of the galaxy are shown, as is the average distribution. The centre of the galaxy was taken to be the position of the radio continuum source (see Table 2). The radial density profile shows a central depression, and peaks at a surface density of 8.6 $M_{\odot}$ pc^{-2} and 9.1 $M_{\odot}$ pc^{-2} at radii of 25 kpc and 45 kpc, on the approaching and receding sides of the galaxy, respectively. The H I radius, measured at the position where the average radial density of the H I profile drops to 1 $M_{\odot}$ pc^{-2}, is ∼66 kpc.

3.1.3 HI rotation curve

The H I rotation curve was measured using the envelope-tracing method (Sofue 1996, 1997), a method known to provide reliable rotation curves for highly inclined galaxies (Olling 1996). The rotation velocity is given by:

$$V_{\mathrm{rot}} = (V_{\mathrm{t}} - V_{\mathrm{sys}})/\sin i - (\sigma_{\mathrm{obs}}^2 + \sigma_{\mathrm{ISM}}^2)^{1/2} \qquad (1)$$

where σ_{obs} is the velocity resolution and σ_{ISM} is the velocity dispersion of the interstellar gas. We adopt a velocity dispersion of 7 km s^{-1} (Stark & Brand 1989; Malhotra 1994). The terminal velocity, V_{t}, is the velocity at which the intensity becomes:

$$I_{\mathrm{t}} = [(0.2 I_{\max})^2 + I_{3\sigma}^2]^{1/2} \qquad (2)$$

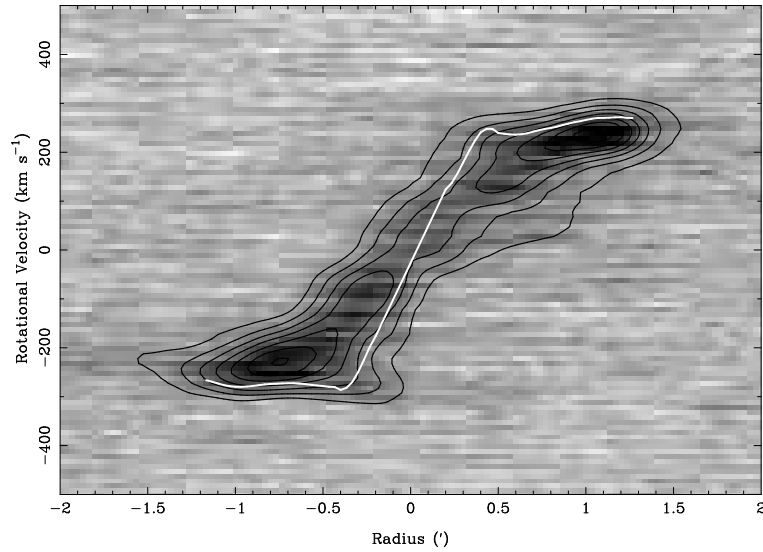where $I_{\max}$ and $I_{3\sigma}$ are the maximum intensity and 3σ intensity levels, respectively.

Figure 5. H I position-velocity (*pv*) diagram along the major axis ($PA = 285°$) of HIZOA J0836–43 using the combined H I data set with an angular resolution of $20''$. The white line gives the H I rotation curve as shown in Fig. 8. Contours represent intensity levels of 2–8σ, where $\sigma = 1.14$ mJy beam^{-1}, and are measured after smoothing the *pv*-diagram by a Gaussian kernel of width 2.
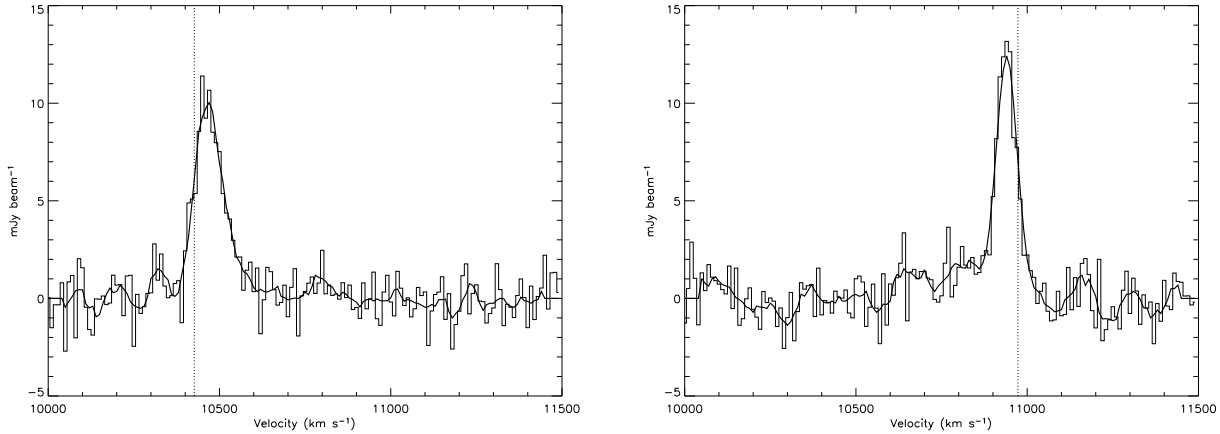

Figure 6. Sample H I velocity profiles of HIZOA J0836–43 obtained from the major-axis *pv*-diagram at offsets of –0.9′ and 1.0′. Dotted lines represent the rotation velocity measured for each slice. Both the unsmoothed and the Savitzky-Golay smoothed profiles are shown for comparison.

To measure V_t, we first used the KARMA package KPVS-LICE to create a position-velocity (*pv*) diagram along the major axis of the galaxy (using $PA = 285°$), shown in Fig. 5. We then plotted as a function of velocity the intensity at a given radius along the major axis. Because of the relatively low S/N, we smoothed the profiles using a Savitzky-Golay smoothing filter with a width of 10 pixels (Press et al. 1992) before measuring $I_{\max}$ and the velocity at which $I = I_t$. Fig. 6 illustrates the effect of this smoothing on two of the velocity profiles, as well as the resulting rotation velocity measured for each slice. After measuring the rotation velocity at each offset, we smoothed the rotation curve by the beam size. Because the image resolution limits the reliability of the central rotation curve derived using the envelope-tracing method (Sofue 1996), we excluded from our rotation curve measurement a central region equal to the beam diameter. We then connected the two sides of the curve with a

line, although we caution that this shape is not necessarily representative of the true central rotation curve.

The inclination-corrected rotation curve is shown in Fig. 7; it is also overlaid onto the *pv*-diagram shown in Fig. 5. The rotation velocity reaches a local maximum at a radius of ∼15 kpc, drops slightly, and then rises to the inclination-corrected value of 304 km s^{-1}, remaining relatively flat and symmetric out to a radius of ∼50 kpc. The rotation velocity is in close agreement with that implied by the inclination-corrected 50% velocity width (310 km s^{-1}).

3.2 Infrared observations and photometry

The 4-m Anglo-Australian Telescope (AAT) was used to obtain K_s- and H-band images of HIZOA J0836–43 on 2003 April 9, with exposure times of 660 s and 420 s, respectively, and $1''.8 - 2''.0$ seeing. The final images were made by random dithering of 11 K_s-band images and 7 H-band images in a
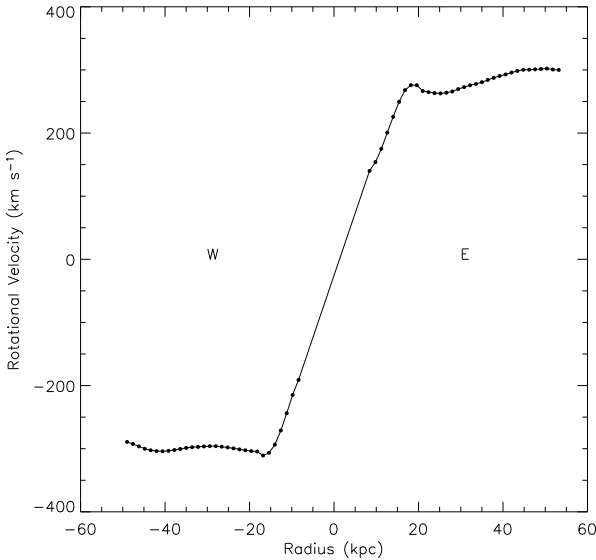
Figure 7. H I rotation curve of HIZOA J0836–43 derived using the envelope-tracing method.

$\pm 30''$ box. The positions were calibrated using the KOORDS tool in Karma (Gooch 1996), with a DENIS (Epchtein 1997) image of the same field serving as the reference. The DENIS positions are accurate to better than $1''$.

To obtain accurate photometry of the three galaxies in the crowded fields, we first measured and subtracted all of the stars in the field using the IRAF[2] package KILLALL (see Woudt et al. 2005 for a detailed description). The resulting star-subtracted images are shown in Fig. 8 and Fig. 9. We then used the IRAF task ELLIPSE to derive the integrated magnitudes for all three galaxies; they are shown in Fig. 10 and listed in Table 4 together with data from 2MASS and DENIS. We calibrated the AAT images by comparing the AAT point sources, measured as described above, with sources from the 2MASS Point Source Catalog[3].

The radial surface brightness profiles are shown in Fig. 11. As in Beijersbergen et al. (1999) and Galaz et al. (2002), we simultaneously fit the surface brightness data by two exponential profiles, taken to be the bulge and disk components of the galaxy:

$$\mu(r) = \mu_\circ + 1.086 \times \frac{r}{h} \quad \text{mag arcsec}^{-2} \qquad (3)$$

The surface brightness profile parameters are given in Table 3. We used a geometric (multiplicative) step when measuring the surface brightness profile because such a step does not oversample the outer regions, where little flux is detected. Changing to a linear step gives more weight to the

---

disk component and tends to brighten the disk central surface brightness by an average of 0.7 mag and decrease the disk scale height by $\sim 1''$; the change in the bulge parameters is less significant. A linear step also changes the central extinction-corrected (H-$K_{\rm s}$) colours of the bulge and the disk, from 0.41 and 0.50, to 0.44 and 0.34, respectively. When corrected for the inclination of the galaxy assuming no optical depth, the face-on central surface brightness of the disk and bulge components, $\mu_{\rm fo} = \mu_{\rm i} - 2.5 \log(\cos i)$, becomes fainter by 1 mag. This correction is almost exactly cancelled by the K-band extinction correction.

The bulge of HIZOA J0836–43 has a central observed surface brightness of $\mu_\circ = 14.81$ (15.70) mag arcsec^{-2} in the $K_{\rm s}$- (H -) band images and a scale length of $h \sim 2.5''$ or 1.7 kpc. The disk of HIZOA J0836–43 has a central observed surface brightness of $\mu_\circ = 16.75$ (17.74) mag arcsec^{-2} and a scale length of $h \sim 7''$ or 4.7 kpc. The bulge-to-disk ratio, B/D, calculated from the surface brightness profile fits, is 0.80 (0.83) in the $K_{\rm s}$- (H -) band.

The integrated infrared magnitudes are given in Table 4, together with the infrared properties measured in 2MASS, and DENIS. The formal statistical error on all AAT magnitudes listed in Table 4 is ~ 0.01 mag; this error does not include potential systematic errors introduced during image processing. The inclination of HIZOA J0836–43, measured from the surface brightness fits to the star-subtracted images, $i \sim 66°$, was calculated assuming an intermediate value of $p = c/a = 0.15$ (see Haynes & Giovanelli 1984).

4   THE GALAXY HIZOA J0836–43

The overall properties of the galaxy HIZOA J0836–43, derived from our H I and infrared data, are summarised in Table 2. Below, we discuss the H I and dynamical mass of HIZOA J0836–43, along with its star formation rate, morphology, NIR colours, location on the Tully-Fisher relation, and environment.

4.1   The H I and dynamical mass

The H I flux density of HIZOA J0836–43 as obtained from the Parkes HIZOA data is $F_{\rm HI} = 13.2 \pm 1.3$ Jy km s^{-1}, similar to the value of 14.5 ± 0.7 Jy km s^{-1} measured with the ATCA in 750D array (see Table 1), suggesting that little (if any) H I emission was resolved out by the interferometer in this configuration. We adopt the ATCA value to estimate an H I mass of $M_{\rm HI} = 7.5$ (± 0.3) $\times 10^{10}$ $M_\odot$. Assuming the other two galaxies in the field (see Figs. 3 and 8) lie at the same distance as HIZOA J0836–43, we estimate an upper limit to their individual H I masses of $\sim 5 \times 10^9$ $M_\odot$.

The H I diameter of HIZOA J0836–43 is at least $3'$, corresponding to 120 kpc. Our analysis of the H I radial density profile indicates a face-on radius of 66 kpc, at a surface density of 1 $M_\odot$ pc^{-2}. Using the H I radius and the inclination-corrected rotational velocity of $v_{\rm rot}^i = 304$ km s^{-1}, we derive a total enclosed dynamical mass of $M_{\rm dyn} = 1.4 \times 10^{12}$ $M_\odot$. The ratio of H I mass to dynamical mass is 0.053.

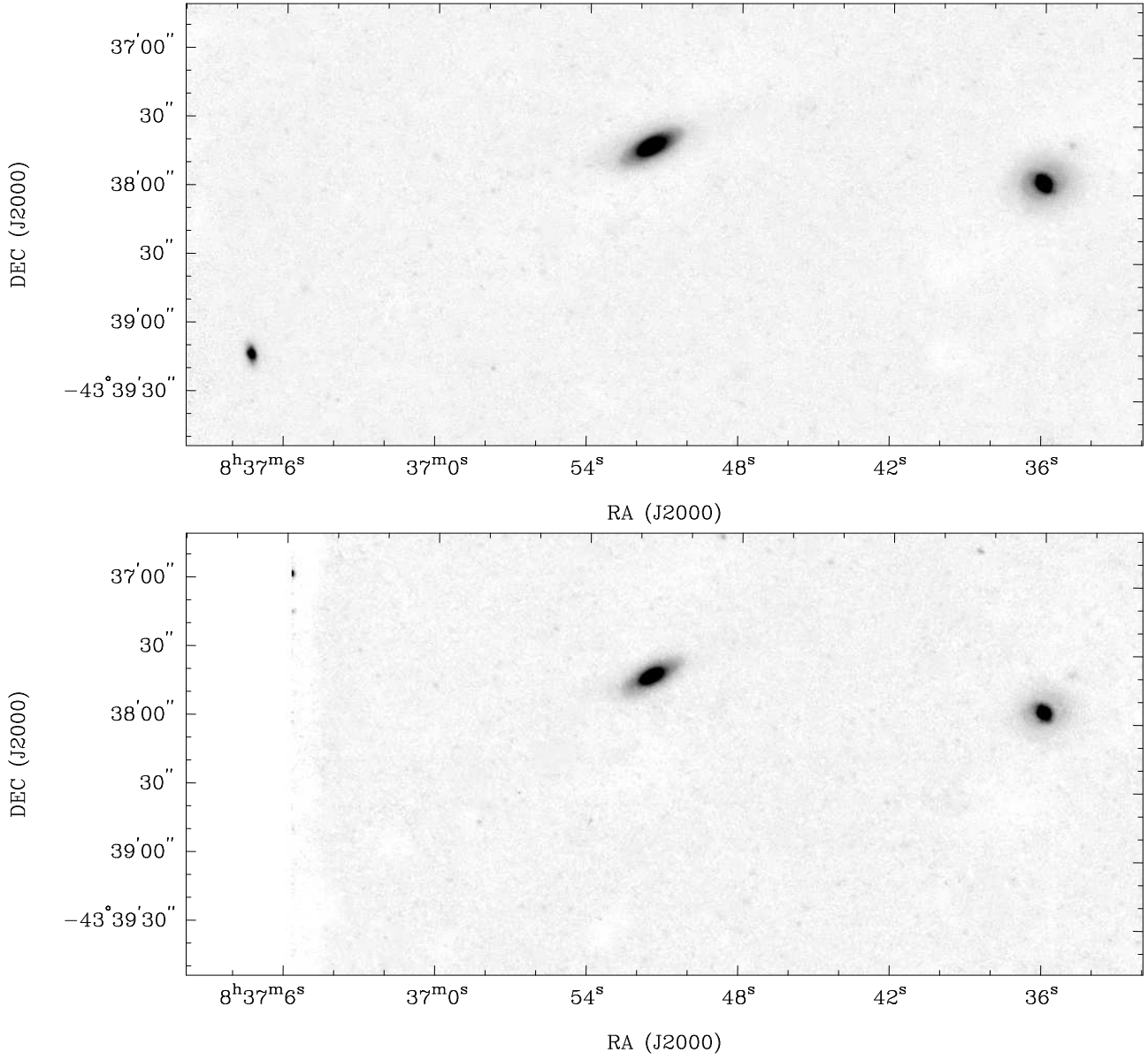**Figure 8.** Star-subtracted AAT K_s-band image (top) and H-band image (bottom) of HIZOA J0836–43 and neighbouring galaxies.
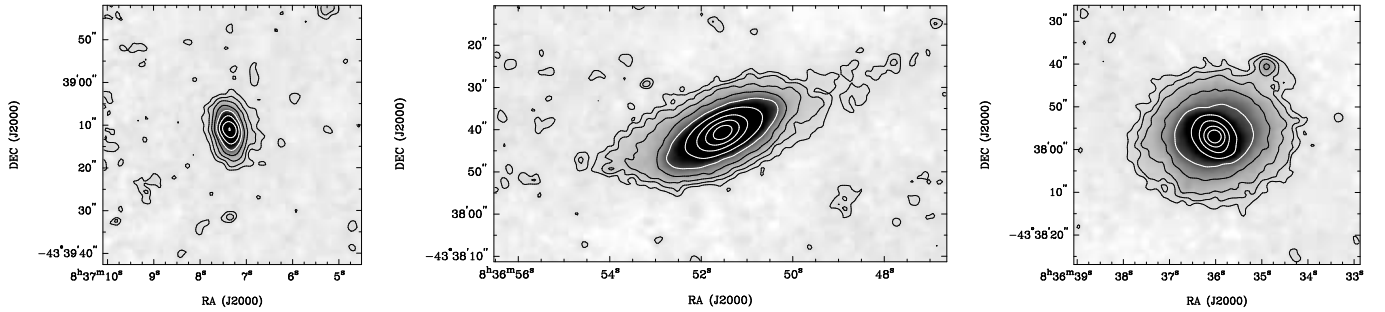

Figure 9. Star-subtracted AAT K_s-band images of 2MASX J08370723–4339137 (left), HIZOA J0836–43 (middle) and 2MASX J08363600–4337556 (right). The contour levels are 30, 80, 160, 320, 640, 1280, 2560, 5120, and 10240 units. The images were convolved with a 1″.5 Gaussian.
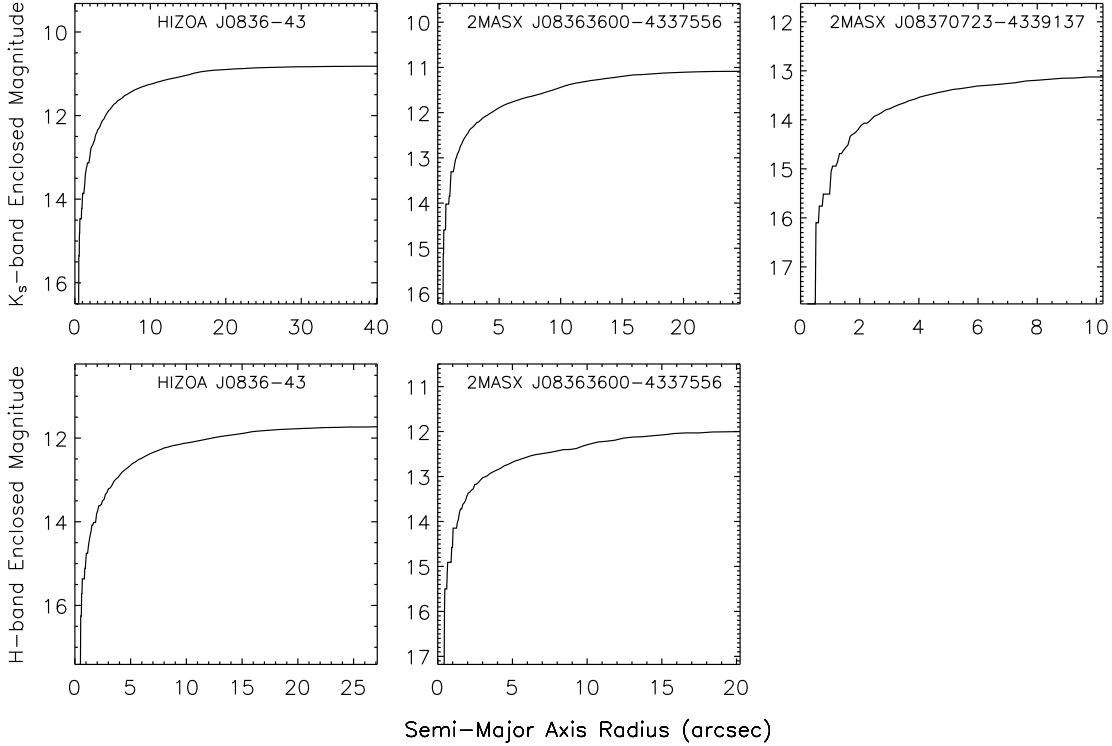
Figure 10. Enclosed AAT K_s-band (top) and H-band (bottom) elliptical magnitudes as a function of semi-major axis radius (see also Table 4). Magnitudes have not been corrected for extinction.

4.2 Star formation rate

The 20-cm radio continuum data reveal a slightly extended source coincident with HIZOA J0836–43 (see Fig. 3). The source has a total flux density of $\sim$24 mJy, a deconvolved size of $11'' \times 7''$, and a major axis position angle of $120°$. The centre position of the radio continuum source is α, δ(J2000) = 08:36:51.54, –34:37:41.5 ($\pm 0.1''$). Using the relation calibrated by Bell (2003), we calculate a star formation rate (SFR) of 35 $M_\odot$ yr^{-1}. Assuming that $M_{\mathrm{gas}} = 1.4 \times M_{\mathrm{HI}}$, the gas consumption time, M_{gas}/SFR, for HIZOA J0836–43 is 3 Gyr and is therefore quite typical for spiral galaxies (Kennicutt et al. 1994).

The far-infrared (FIR) 60 μm flux density of HIZOA J0836–43 from the High Resolution Infrared Astronomical Satellite (IRAS) Atlas (Cao et al. 1997) confirms that star formation, and not AGN activity, is responsible for the radio continuum emission. Although HIZOA J0836–43 is clearly detected at 60 μm (and marginally detected at 100 μm), source confusion prevents measurement of an accurate flux. We instead place conservative upper and lower limits on the 60 μm flux density by summing the galaxy emission inside an elliptical aperture and subtracting both the low and high extremes of the local sky; we measure a 60 μm flux density of $\sim 1.5 - 4.8$ Jy.

From the FIR 60 μm flux density limits, the radio/infrared correlation for star-forming galaxies and radio-quiet AGN (Yun, Reddy, and Condon 2001) predicts radio luminosities that are a factor of $0.5 - 1.6$ times that observed. The observed radio luminosity therefore exceeds the expected luminosity by at most a factor of 2, falling far below the factor of 5 required for 'radio-excess' AGN (Yun et al. 2001, Drake et al. 2003), and confirming that the radio continuum emission is dominated by star formation.

While there is no sign of any radio continuum emission at the position of the galaxy 2MASX J08363600–4337556, west of HIZOA J0836–43, the smaller galaxy to the southeast of HIZOA J0836–43, 2MASX J08370723–4339137, is detected with a 20-cm flux density of $\sim$1 mJy (see bottom panel of Fig 3). The rms in the continuum image is $\sim$0.1 mJy beam^{-1}.

4.3 Morphology and colours

The morphology of HIZOA J0836–43 remains a puzzle. The H I observations show a rapidly rotating, very gas-rich galaxy with — as seen in the previous section — a high star formation rate, indicative of an Sb or Sc galaxy (Roberts & Haynes 1994, Kennicutt 1992). In addition, the $M_{\mathrm{HI}}/M_{\mathrm{dyn}}$ ratio of HIZOA J0836–43 appears typical for Sb–Sc galaxies, but would be within the observed range of values for any galaxy type (Roberts & Haynes 1994). Visual examination of the AAT K_s-band image of HIZOA J0836–43 (Fig. 3), however, and the analysis of its surface brightness profile (Fig. 11 and Table 3), reveal a distinct bright bulge ($\sim$2 kpc) and an extended smooth disk ($\sim$5 kpc) that can be traced along the major axis out to a radius of $\sim$13.4 kpc (at 20 mag arcsec^{-2}). Comparison with the NIR Galaxy Morphology Atlas of Jar-
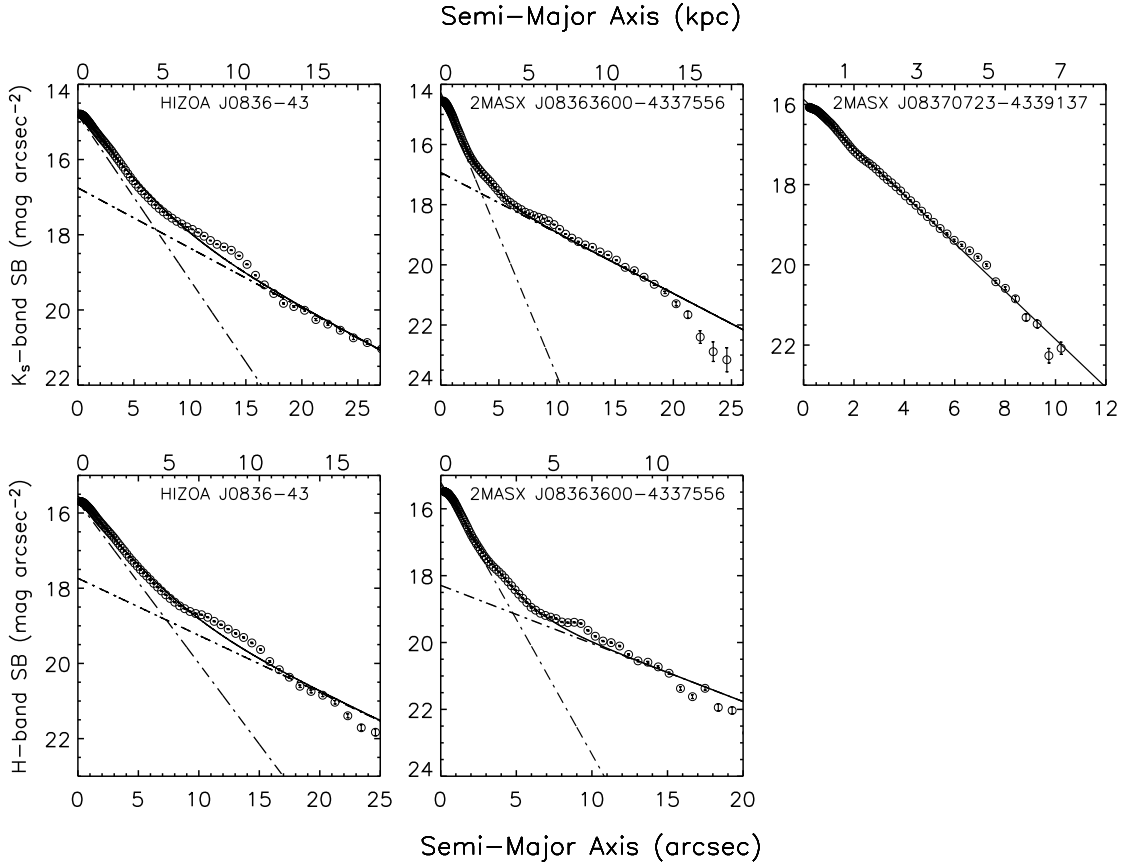
Figure 11. Observed AAT K_s- and H-band surface brightness (SB) profiles. The profiles of HIZOA J0836–43 and 2MASX J08363600–4337556 were simultaneously fit by two exponential profiles, given by the dot-dashed lines. The solid line shows the sum of the two fits. The profile of the third galaxy, 2MASX J08370723–4339137, was fit by a single exponential profile.

rett (2000) leads to the conclusion that HIZOA J0836–43, with its dominant bulge and smooth bulge-to-disk transition, is more likely to be a bright S0 to Sa galaxy than an Sb or Sc. NIR extinction from the Galactic Plane, however, is likely to obscure the disk, causing HIZOA J0836–43 to appear anomalously early in type. Using the NIR positions of HIZOA J0836–43 and its companions, we identify highly obscured optical counterparts in the DSS2 R-band images, but the image resolution is insufficient to provide any details about their morphologies.

The extinction-corrected NIR colours of HIZOA J0836–43, presented in Table 5, are consistent with expectations for normal bright galaxies ($J - K_s = 1^{m}\!\!.0$, $H - K_s = 0^{m}\!\!.27$, and $J - H = 0^{m}\!\!.73$), but provide little morphological information as only late-type spirals (Sd – Sm) deviate from the overall mean (Huchra et al. 2000; Jarrett et al. 2003). The AAT $(H - K_s)^{o}_{5''}$ values of $0^{m}\!\!.39$ and $0^{m}\!\!.34$ for HIZOA J0836–43 and its larger companion, 2MASX J08363600–4337556, lie on the high side of the range for normal 2MASS galaxies; the same colours determined from the 2MASS magnitudes lie on the low side ($0^{m}\!\!.23$ and $0^{m}\!\!.15$). We use the $5''$ colours instead of the total colours because the former are less likely to be affected by extinction and star-subtraction. The $(J - K_s)$ colour of the small galaxy, 2MASX J08370723–4339137, lies well above the mean, which might be indicative of a late type

spiral. In addition, comparison of DENIS central and mean $(I - K_s)$ colours suggests that the total stellar populations of HIZOA J0836–43 and 2MASX J08363600–4337556 are bluer than that of the bulges that dominate the light within $7''$.

As shown by Jarrett et al. (2003), NIR effective surface brightnesses brighten with decreasing morphological type, T. After extinction correction, the mean effective surface brightnesses listed in Table 2 suggest that HIZOA J0836–43 is of early type, in the range E (elliptical) to Sa, although the H and K_s surface brightnesses lie within the rms uncertainties for types as high as Sb. The face-on companion 2MASX J08363600–4337556 also seems of early type, in the range E to Sa, and the third small companion 2MASX J08370723–4339137 seems to be a spiral between Sab and Sc, in agreement with its S-shaped structure and the indication of star formation (see the bottom panel of Fig. 3).

As a final test of morphology, we compare the central surface brightness in the J- and K_s-band with the total K_s magnitude. According to Jarrett (2000), SA0/S0 galaxies follow a linear relation of the form $J_{5''} = 0.8K_s + 8.8$, and $K_{5''} = 0.8K_s + 7.8$. Spiral galaxies of later type (T) follow the same slope but with an increasing offset towards fainter magnitudes with increasing T, while ellipticals generally lie below this regression. The $J_{5''}$ and the $K_{5''}$ relations again suggests that the massive spiral galaxy HIZOA J0836–

43 is an S0 (lenticular) or Sa galaxy. The larger companion, 2MASX J08363600–4337556, also seems of early type. For the small spiral-like galaxy, 2MASX J08370723–4339137, the test however, also indicates an early type which it clearly is not. This may be due to the fact that this galaxy is very small and hardly resolved; the above relation is valid only for well resolved galaxies.

The NIR morphology, colours, and magnitudes therefore indicate that HIZOA J0836–43 may be an S0 or Sa galaxy, although we caution that extinction is likely to obscure the disk, causing the bulge to dominate the photometry and therefore bias our results towards early morphological types. Given its enormous H I content, it may at first seem contradictory that HIZOA J0836–43 could be a lenticular galaxy. However, some lenticulars are known to contain a large amount of neutral gas. Such galaxies include low surface brightness lenticulars, of which the edge-on S0 galaxy NGC 5084 (Gottesman & Hawarden 1986) is a typical example (see also O'Neil et al. 2004), as well as high surface brightness lenticulars (Eder et al. 1991). For many S0 galaxies — in particular polar ring galaxies — the gas seems to be due to recent accretion events. Other H I-rich lenticulars (e.g., NGC 5084), however, have H I disks that are aligned with their optical counterparts as well as similar gas and stellar kinematics, suggesting that the H I is intrinsic in origin.

4.4 NIR Tully-Fisher relation

In order to test whether HIZOA J0836–43 lies on the Tully-Fisher relation, we compare our data to the NIR (R, I, H, K_s) Tully–Fisher relations as calibrated by Macri (2001). These relations, calibrated for both total and isophotal magnitudes (20 mag/arcsec^2), exhibit slopes with small dispersions ($0.^{\rm m}19 - 0.^{\rm m}22$).

We list in Table 6 the absolute magnitudes estimated from Macri's Tully-Fisher relations (using the inclination-corrected 20% velocity width, $\log w_{20}^i = 2.82$) and the extinction-corrected, absolute magnitudes obtained from AAT, 2MASS and DENIS photometry[4]. The offsets between the predicted and measured magnitudes, as well as the slopes and intercepts of the regressions $M = a + b(\log w_{20}^i - 2.5)$, are also listed. For all bands, HIZOA J0836–43 lies on the NIR TF relation, never deviating by more than 1σ, suggestive of a normal galaxy at the extreme high-mass end of the NIR TF relation.

4.5 The environment

Does HIZOA J0836–43 form part of a cluster or a group that allowed it to grow to its current dimensions through the accretion of or merging with satellite galaxies, or does it reside in a low-density environment where it remained undisturbed by galaxy interactions? Unfortunately, the study of the environment of HIZOA J0836–43 is made difficult by its location behind the plane of the Milky Way and behind the Vela

---

[4] The internal extinction was corrected according to Masters et al. (2003) using $A_\lambda = c_\lambda \log(a/b)$, with $c_\lambda = 1.16, 0.39, 0.26$ for I, J, K_s, respectively, where (a/b) is the major-to-minor axis ratio.

SNR. With optical extinctions of $\sim$10 magnitudes, the detection of even the intrinsically most luminous galaxies at the distance of HIZOA J0836–43 is nearly impossible. Although NIR surveys are less affected by extinction than optical surveys, they are hindered by confusion. Galaxy recognition fails completely in regions where the density of stars with $K \leq 14.^{\rm m}0$ surpasses $\log N = 4.00(\square)^\circ$, and HIZOA J0836–43 (with $\log N = 3.96$) lies extremely close to this so-called "NIR Zone of Avoidance" (see Kraan-Korteweg 2005).

Nevertheless, we attempt to explore the environment of HIZOA J0836–43 by studying all extended sources in the 2MASX catalogue that lie within (1) a square degree around HIZOA J0836–43 and (2) within a circle of radius $1.^\circ2$, the equivalent of an Abell radius at the distance of HIZOA J0836–43. With the exception of two small pockets of extreme dust, the extinction A_K in this area ranges from $0.^{\rm m}6$ to $1.^{\rm m}4$. Subtracting the latter from the nominal 2MASS completeness limit of $K_s \leq 13.^{\rm m}5$ (Jarrett 2000), we expect our extended source search to be complete to $K_S^\circ \lesssim 12.^{\rm m}1$ in extinction-corrected magnitude, ignoring confusion. To exclude Galactic sources from this sample, we visually inspect all 2MASX objects brighter than $K_S^\circ \leq 12.^{\rm m}0$.

In the central square degree, there are 14 2MASX extended sources with $K_S^\circ \leq 12.^{\rm m}0$. Of these, one was rejected, leaving 10 certain galaxies and 3 possible galaxies. The galaxy density of the studied region is therefore at least a factor of 5 higher than the mean density of 2MASS galaxies with $K_S \leq 12.^{\rm m}0$ and $|b| \geq 25^\circ$, 1.8 gal/$(\square)^\circ$ (Jarrett 2004; Jarrett 2005, priv. comm.), although the redshift of the overdensity remains undetermined. Within the Abell radius, 29 extended sources have $K_S^\circ \leq 12.^{\rm m}0$; of these, six were rejected, leaving 18 certain galaxies plus 5 possible galaxies. The resulting galaxy density in the Abell radius therefore also exceeds the mean, by a minimum factor of 2–3.

To investigate the effect of confusion on the overdensity, we repeated the study for completeness limits of $K_S^\circ \leq 11.^{\rm m}5$ and $11.^{\rm m}0$. The mean 2MASX densities (away from the Galactic Plane) are 0.85 and 0.43 gal/$(\square)^\circ$, respectively. Although the statistics are poorer, we find galaxy densities in the square degree around HIZOA J0836–43 of $7-10$ and $5-8$ gal/$(\square)^\circ$, respectively, indicating even higher overdensities than for the $K_S^\circ \leq 12.^{\rm m}0$ completeness limit. The overdensity within the Abell radius remains approximately the same. It therefore appears that HIZOA J0836–43 lies in an overdense region — at least projected on the sky — with the galaxy density increasing in the central square degree and becoming more prominent for the brightest objects.

Although we do not have redshifts for the individual 2MASS galaxies, we estimate the redshift of the deduced galaxy overdensity, and its relation to the redshift of HIZOA J0836–43, $z = 0.036$, by considering the large-scale structure of 2MASS galaxies in several photometric redshift intervals, as determined by Jarrett (2004). Prominent in the slice $0.04 < z < 0.05$, but also visible in the $0.03 < 0.04$ slice, is a filamentary supercluster-like feature that crosses the Galactic Plane at the position of HIZOA J0836–43 and that points towards the Shapley concentration. This feature could explain the projected overdensity of galaxies around HIZOA J0836–43. In addition, a large fraction of the 2MASS galaxies seem to be of similar size and appearance as HIZOA J0836–43 (taking absorption effects into account), and are therefore likely to lie at similar redshifts.

Finally, we checked for H I-rich neighbours to HI-ZOA J0836–43 by observing a $2° \times 2°$ area around it with the Parkes multibeam system in 2004 November. The integration time was $4\times$ longer than for the deep Parkes H I ZOA survey, and $20\times$ longer than for HIPASS. The central velocity was set to $10\,000$ km s^{-1}; the 64 MHz bandwidth give velocity coverage from 3300 km s^{-1} to 16 700 km s^{-1}. A careful inspection of the deep H I data cube did not reveal any additional galaxies. Given an rms of $\gtrsim 3$ mJy, the 5σ H I-mass limit for a detection at $D = 148$ Mpc is $\gtrsim 1.5\times10^{10}\,M_\odot$ (assuming a top-hat with a velocity width of 200 km s^{-1}). Areas with strong continuum emission are adversely affected by a baseline ripple which increases the noise by a factor 2–3.

5   COMPARISON WITH OTHER H I-MASSIVE GALAXIES

The four most H I-massive galaxies known are HIZOA J0836–43, UGC 4288 (O'Neil et al. 2004), UGC 1752 (Matthews et al. 2001), and, of course, Malin 1 (Bothun et al. 1987). The latter three are low-surface brightness (LSB) galaxies at luminosity distances of 433, 249 and 351 Mpc, respectively. Their H I properties are summarised in Table 7.

The galaxy UGC 4288 was classified as Sdm by Schombert & Bothun (1988) and as S0 by O'Neil et al. (2004). Optical images show a bright bulge and faint spiral structure, suggesting that UGC 4288 is likely to be of late type. The galaxy UGC 1752, which was classified as SAcd by de Vaucouleurs et al. (1991), looks remarkably similar to UGC 4288, suggesting the latter is also of late type. Malin 1 has a prominent bulge, with the properties of a bright elliptical galaxy, and a low-surface brightness disk that is barely detectable. The galaxy HIZOA J0836–43 is highly obscured in the optical and its morphological type is unknown. While our analysis of its NIR colours slightly favour an early-type morphology, extinction is likely to obscure the disk, causing the measurements to be dominated by the prominent bulge. The surface brightness analysis gives $B/D \sim 0.8$, a value slightly higher than that seen in LSBs ($B/D = 0.56 \pm 0.07$; Sprayberry et al. 1995), but roughly consistent with that of spiral galaxies ($B/D = 0.61 \pm 0.20$; Kent 1985). The extinction- and inclination-corrected central K_s-band surface brightness of the disk ($\mu_\circ = 16.9$ mag arcsec^{-2}) falls well short of the typical LSB cut, 18.0 mag arcsec^{-2}, indicating that unlike the other H I-massive galaxies listed above, HIZOA J0836–43 is not an LSB galaxy.

The H I diameters of all four galaxies are huge: Malin 1 ($\sim2'.5$ or 220 kpc), UGC 1752 ($\sim2'$ or 130 kpc), and HIZOA J0836–43 ($\sim3'$ or 120 kpc). No H I diameter has been measured for UGC 4288 (yet) but its optical extent of $\sim1'$ (or 100 kpc) is likely to be a lower limit. All four galaxies also have high rotational velocities; while their inclination angles are rather uncertain (Malin 1: $i \approx 45°$, UGC 1752: $i \approx 0°$; UGC 4288 $i \approx 40°$; HIZOA J0836–43: $i \approx 66°$), we deduce rotational velocities of $\gtrsim 200$–300 km s^{-1} from the velocity width of their H I profiles (see Table 7). We note that UGC 4288, UGC 1752, and Malin 1 appear to lie in very low density environments. Their lack of tidal interactions may have played a role in preserving such large H I masses and diameters.

It therefore appears that the four H I-massive galaxies discussed above are similar in their extreme H I masses, large disks, and high rotational velocities. It is possible, however, that HIZOA J0836–43 differs from the others in its high SFR, high surface brightness disk, potentially overdense environment, and morphology. A more detailed comparison of these galaxies will follow in Koribalski et al. (in preparation).

6   CONCLUSIONS

HIZOA J0836–43 is a remarkable galaxy. Its enormous H I mass ($M_{HI} = 7.5$ (±0.3) $\times10^{10}\,M_\odot$), large H I velocity width ($w_{20} = 610 \pm 9$ km s^{-1}), and paucity of optical information due to its location in the Zone of Avoidance raises numerous questions about its environment, morphology and overall kinematics. ATCA H I observations reveal a very extended, highly-inclined H I disk (see Fig. 2) and a surprisingly regular velocity field. We measure an H I diameter of at least $3'$ which corresponds to a physical size of ~120 kpc. For comparison, the H I diameter of Malin 1, the largest disk galaxy known so far, is ~220 kpc (Pickering et al. 1997, Matthews et al. 2001).

The H I distribution of HIZOA J0836–43 is slightly asymmetric (with more H I gas on the eastern side of the galaxy) and reveals a central depression. It also shows a gradually changing major axis position angle which decreases from $PA \sim 290°$ in the inner region to nearly $270°$ in the outermost region. This change, which is most pronounced on the eastern side of the galaxy, is indicative of a gentle warp.

The H I velocities observed in HIZOA J0836–43 range from ~ 10400 to 11000 km s^{-1}, indicating an inclination-corrected rotation velocity of 304 km s^{-1} and consequently, a large dynamical mass and dark matter content. HIZOA J0836–43 falls on the NIR Tully-Fisher relationship, indicating that it is a normal rotating galaxy. We note that the equal velocity contours are nearly straight and do not resemble a typical spider diagram. A detailed analysis of the galaxy kinematics is limited by the relatively low angular resolution.

NIR data from the AAT indicate that HIZOA J0836–43 has a both a prominent bulge and an extended disk, and NIR colours point to an early type (S0-Sa) morphology, although colours from AAT, 2MASS, and DENIS may be dominated by the bulge component due to obscuration of the disk. The high star formation rate measured from the radio continuum and IRAS data, $SFR \sim 35\,M_\odot$ yr^{-1}, suggests a later morphological type of Sb or Sc. A study of the local environment of HIZOA J0836–43, using sources from the 2MASX extended source catalogue, indicate that HIZOA J0836–43 may lie in an overdense region, possibly part of a supercluster-like filament.

There are currently very few galaxies known with H I masses of $\sim 10^{11}\,M_\odot$; these are HIZOA J0836–43, UGC 1752, Malin 1, and UGC 4288 (in order of increasing distance; see Table 7). Accurate H I mass estimates can be difficult for such distant galaxies because of flux calibration uncertainties and low signal to noise. In addition, single-dish H I spectra are often fitted with multiple-order baselines which result in large flux uncertainties due to the very wide H I velocity profiles of these supermassive galaxies. We have obtained

deep H I spectra of the LSB galaxies Malin 1 and UGC 4288 with the Parkes 64-m telescope and will report the results in Koribalski et al. (in preparation) together with a comprehensive comparison of the most H I-massive galaxies known from the literature. Constraining the number of massive galaxies in the Universe is necessary if we are to better understand the high-mass end of the galaxy mass and luminosity functions, and studying the properties of such galaxies provides a test of current galaxy formation scenarios in their most extreme limits.

ACKNOWLEDGMENTS

REFERENCES

Barnes, D.G. et al., 2001, MNRAS, 322, 486
Beijersbergen, M., de Blok, W.J.G., van der Hulst, J.M., 1999, A&A, 351, 903
Bell, E.F., 2003, ApJ, 586, 794
Blanton, M.R. et al., 2003, ApJ, 592, 819
Bothun, G.D., Impey, C.D., Malin, D.F., Mould, J.R., 1987, AJ, 94, 23
Cao, Y., Terebey, S., Prince, T.A., Beichman, C.A., 1997, ApJS, 111, 387
Cole, S., Lacey, C.G., Baugh, C.M., Frenk, C.S., 2000, MNRAS, 319, 168
Colina, L., Bohlin, R., 1997, AJ, 113, 1138
Croton, D.J. et al., 2006, MNRAS, 365, 11
Davies, J.I., Sabatini, S., Roberts, S., 2004, PASA, 21, 360
Donley, J.L. et al., 2005, AJ, 129, 220
Drake, C.L., McGregor, P.J., Dopita, M.A., van Breugel, W.J.M., 2003, AJ, 126, 2237
Eder, J., Giovanelli, R., Haynes, M.P., 1991, AJ, 102, 572
Epchtein, N., 1997, in Garzon, F. et al., eds, 2nd DENIS Euroconference, The impact of large scale near-infrared surveys. Dordrecht, Kluwer, 15
Fixsen, D.J., Cheng, E.S., Gales, J.M., Mather, J.C., Shafer, R.A., Wright, E.L., 1996, ApJ, 473, 576
Foerster Schreiber, N.M. et al., 2004, ApJ, 616, 40
Galaz, G., Dalcanton, J.J., Infante, L., Treister, E., 2002, AJ, 124, 1360
Gooch, R., 1996, in Jacoby, G.H., Barnes,J., eds, ASP Conf. Ser. Vol. 101, Astronomical Data Analysis Software and Systems V. Astron. Soc. Pac., San Francisco, p. 80
Gottesman, S.T., Hawarden, T.G., 1986, MNRAS, 219, 759
Haynes, M.P, Giovanelli, R., 1984, AJ, 89, 758

Henning, P.A. et al., 2000, AJ, 119, 2686
Henning, P.A., Kraan-Korteweg, R.C., Staveley-Smith, L., 2005, in Fairall, A.P., Woudt, P.A., eds, ASP Conf. Ser. Vol. 329, Nearby Large-Scale Structures and the Zone of Avoidance. Astron. Soc. Pac., San Francisco, p. 199
Huchra, J.P., Mader, J., Schneider, S.E., Skrutskie, M.F., Jarrett, T.H., Chester, T., Cutri, R., 2000, in Kraan-Korteweg, R.C., Henning, P.A., Andernach, H., eds, ASP Conf. Ser. Vol. 218, Mapping the Hidden Universe. Astron. Soc. Pac., San Francisco, p. 101
Impey, C.D., Bothun, G., 1989, ApJ, 341, 89
Jarrett, T.H., 2000, PASP, 112, 1008
Jarrett, T.H., 2004, PASA, 21, 396
Jarrett, T.H., Chester, T., Cutri, R., Schneider, S., Skrutskie, M., Huchra, J.P., 2000, AJ, 119, 2498
Jarrett, T.H., Chester, T., Cutri, R., Schneider, S.E., Huchra, J.P., 2003, AJ, 125, 525
Kauffmann, G., White, S.D.M., Guiderdoni, B., 1993, MNRAS, 264, 201
Kay, S.T., Pearce, F.R, Frenk, C.S., Jenkins, A., 2002, MNRAS, 330, 113
Kennicutt, R.C., 1992, ApJ, 388, 310
Kennicutt, R.C., Tamblyn, P., Congdon, C.E., 1994, ApJ, 435, 22
Kent, S. M. 1985, ApJS, 59, 115
Klypin, A., Nolthenius, R., Primack, J., 1997, ApJ, 474, 533
Koribalski, B.S. et al., 2004, AJ, 128, 16
Kraan-Korteweg, R.C., 2005, in Roeser, S., ed, Rev. in Modern Astrophysics Vol. 18, From Cosmological Structures to the Milky Way. p. 48
Kraan-Korteweg, R.C., Staveley-Smith, L., Donley, J.L., Koribalski, B.S., Henning, P.A., 2004, in Colless, M., Staveley-Smith, L., Stathakis, R. eds, IAU Symp. 216, Maps of the Cosmos, Astron. Soc. Pac. San Franciso, p. 203
Lucy, L.B., 1974, AJ, 79, 745
Macri, L.M., 2001, PhD Thesis, Harvard University
Malhotra, S. 1994, ApJ, 433, 687
Masters, K.L., Giovanelli, R., Haynes, M.P., 2003, AJ, 126, 158
Matthews, L.D., van Driel, W., Monnier-Ragaigne, D., 2001, A&A, 365, 1
Meyer, M.J. et al., 2004, MNRAS, 350, 1195
Norberg, P. et al., 2002, MNRAS, 336, 907
Olling, R.P., 1996, AJ, 112, 457
O'Neil, K., Bothun, G., van Driel, W., Monnier Ragaigne, D., 2004, A&A, 428, 823
Pickering, T.E., Impey, C.D., van Gorkom, J.H., Bothun, G.D., 1997, AJ, 114, 1858
Press, W.H., Schechter, P., 1974, ApJ, 187, 425
Press, W.H., Teukolsky, S.A., Vetterling, W.T., Flannery, B.P., 1992, Numerical recipes in C : the art of scientific computing, 2nd edition. Cambridge University Press, Cambridge
Roberts, M.S., Haynes, M.P., 1994, ARA&A, 32, 115
Rosenberg, J.L., Schneider, S.E., 2002, ApJ, 567, 247
Schechter, P., 1976, ApJ, 203, 297
Schlegel, D.J., Finkbeiner, D.P., Davis, M., 1998, ApJ, 500, 525
Schombert, J.M., Bothun, G.D., 1988, AJ, 95, 1389
Sofue, Y., 1996, ApJ, 458, 120
Sofue, Y., 1997, PASJ, 49, 17
Sprayberry, D., Impey, C. D., Bothun, G. D., Irwin, M. J., 1995, AJ, 109, 558
Springel, V. et al., 2005, Nature, 435, 629
Stark, A.A., Brand, J., 1989, ApJ, 339, 763
Staveley-Smith, L. et al., 1996, PASA, 13, 243
van der Hulst, J.M., Terlouw, J.P., Begeman, K.G., Zwitser, W., Roelfsema, P.R., 1992, in Worall, D.M., Biemesderfer, C., Barnes, J., eds, ASP Conf. Ser. Vol. 25, Astronomical Data Analysis Software and Systems I. Astron. Soc. Pac., San Francisco, p. 131
de Vaucouleurs, G., de Vaucouleurs, A., Corwin Jr., H.G., Buta,

R.J., Paturel, G., Fouqué, P., 1991, Third Reference Catalogue of Bright Galaxies. Springer Verlag, New York

Warmels, R.H., 1988, A&AS, 72, 427

Wong, I., et al., 2005, MNRAS, submitted

Woudt, P.A., Fairall, A.P., Kraan-Korteweg, R.C., Lucey, J., Schröder, A., Burstein, D., McCall, M.L., 2005, in Fairall, A.P., Woudt, P.A., eds, ASP Conf. Ser. Vol. 329, Nearby Large-Scale Structures and the Zone of Avoidance. Astron. Soc. Pac., San Francisco, p. 147

Yun, M.S., Reddy, N.A., Condon, J.J., 2001, ApJ, 554, 803

Zwaan, M.A. et al., 2003, AJ, 125, 2842

Zwaan, M.A., Meyer, M.J., Staveley-Smith, L., Webster, R.L., 2005, MNRAS, 359, L30

Table 1. Measured H I properties of the galaxy HIZOA J0836–43

Observation	rms [mJy beam^{-1}]	H I flux density F_{HI} [Jy km s^{-1}]	Heliocentric velocity, cz [km s^{-1}]	Velocity width w_{50} [km s^{-1}]	w_{20} [km s^{-1}]	Reference
Parkes ZOA survey	6	13.2 ± 1.3	10706 ± 7	550 ± 14	607 ± 21	here
ATCA	1.2	14.5 ± 0.7	10689 ± 3	566 ± 6	610 ± 9	here
HIPASS	13	15.6 ± 2.9	10710 ± 16	575 ± 32	654 ± 48	HICAT (Meyer et al. 2004)

Note: The uncertainties were calculated following the formulas given in Koribalski et al. (2004) and references therein.

Table 2. A summary of the properties of the galaxy HIZOA J0836–43

Property	Value	Notes
centre position, α, δ(J2000)	$08^{\mathrm{h}}36^{\mathrm{m}}51.54^{\mathrm{s}}$, $-43°37'41''.5$	(a)
heliocentric velocity, v_{hel}	10689 ± 3 km s^{-1}	(b)
CMB velocity, v_{CMB}	10928 ± 3 km s^{-1}	$\cdots$
luminosity distance	148 Mpc	(c)
H I flux density, F_{HI}	14.5 ± 0.7 Jy km s^{-1}	(b)
H I mass, M_{HI}	7.5×10^{10} $M_{\odot}$	(b)
position angle, PA	$285° \pm 15°$	(d)
inclination angle, i	$66° \pm 3°$	(d)
intrinsic rotation velocity, v_{rot}^{i}	304 km s^{-1}	$\cdots$
H I radius (at 1 $M_{\odot}$ pc^{-2})	66 kpc	(e)
total dynamical mass, M_{dyn}	1.4×10^{12} $M_{\odot}$	$\cdots$
absolute magnitude, $M_{K_{\mathrm{s}}}^{c}$	-25.03 mag	(d,f,g)
infrared colour, $(H - K_{\mathrm{s}})$	0.43	(d,f,g)
H I mass to light ratio, M_{HI} / $L_{K_{\mathrm{s}}}$	0.35 $M_{\odot}/L_{\odot}$	(f,g)
H I mass to total mass ratio, M_{HI} / M_{dyn}	0.05	$\cdots$
infrared radius, $(\mu_{K_{\mathrm{s}}}^{c} = 20$ mag arcsec$^{-2})$	13.4 kpc	(d,f)
bulge scale length	1.7 kpc	(d)
disk scale length	4.7 kpc	(d)
star formation rate (SFR)	35 $M_{\odot}$ yr^{-1}	(a)

Notes: (a) from the ATCA 20-cm radio continuum data; (b) from the ATCA 750D array H I line data; (c) assuming $H_0 = 75$ km s^{-1} Mpc^{-1} (see § 3.1.1); (d) from the AAT H- and K_{s}-band data; (e) when viewed face-on; (f) corrected for Galactic extinction (Schlegel et al. 1998); (g) the absolute magnitude of the Sun in K-band is $M_{K,\odot} = 3.31$ mag (Colina & Bohlin 1997).

Table 3. Observed Surface Brightness Profile Parameters

Source	Band	$\mu_{\circ}$ [mag arcsec^{-2}]	Bulge Parameters $\mu_{\circ}$ [mag arcsec^{-2}]	h [$''$]	Disk Parameters $\mu_{\circ}$ [mag arcsec^{-2}]	h [$''$]
HIZOA J0836–43	H	15.55	15.70	2.53	17.74	7.15
	K_{s}	14.65	14.81	2.48	16.75	6.79
2MASX J08363600–4337556	H	15.20	15.27	1.34	18.29	6.25
	K_{s}	14.27	14.37	1.16	16.93	5.40
2MASX J08370723–4339137	K_{s}	15.87	15.87	1.81	$\cdots$	$\cdots$

Note: Magnitudes have not been corrected for foreground extinction, values of which are listed in Table 4.

Table 4. Observed Infrared Parameters

Source	Band	A_λ [mag]	Telescope	r_{20} ["]	r_{eff} ["]	m_{tot}	m_{20}	$m(r<5'')$	$SB(r_{eff})$ [mag arcsec^{-2}]
HIZOA J0836–43	I	4.40	DENIS	$\cdots$	$\cdots$	16.59 ± 0.10	$\cdots$	$\cdots$	$\cdots$
	J	2.05	2MASS	11.2	7.7	13.16 ± 0.13	13.25 ± 0.08	13.99 ± 0.05	18.75
		$\cdots$	DENIS	$\cdots$	$\cdots$	13.17 ± 0.04	$\cdots$	$\cdots$	$\cdots$
	H	1.31	AAT	16.1	6.0	11.73 ± 0.01	11.84 ± 0.01	12.39 ± 0.01	17.77
		$\cdots$	2MASS	20.3	10.8	11.44 ± 0.06	11.81 ± 0.06	12.55 ± 0.03	17.71
	K_s	0.83	AAT	20.2	6.3	10.82 ± 0.01	10.90 ± 0.01	11.52 ± 0.01	17.02
		$\cdots$	2MASS	17.8	9.6	10.84 ± 0.06	11.18 ± 0.06	11.84 ± 0.02	16.86
		$\cdots$	DENIS	$\cdots$	$\cdots$	11.02 ± 0.10	$\cdots$	$\cdots$	$\cdots$
2MASX J08363600–4337556	I	4.27	DENIS	$\cdots$	$\cdots$	17.04 ± 0.08	$\cdots$	$\cdots$	$\cdots$
	J	1.99	2MASS	6.7	5.1	13.37 ± 0.14	13.43 ± 0.10	14.10 ± 0.05	18.81
		$\cdots$	DENIS	$\cdots$	$\cdots$	13.63 ± 0.03	$\cdots$	$\cdots$	$\cdots$
	H	1.27	AAT	11.2	4.5	12.00 ± 0.01	12.22 ± 0.01	12.62 ± 0.01	18.22
		$\cdots$	2MASS	11.6	6.6	11.84 ± 0.08	12.08 ± 0.08	12.76 ± 0.04	17.84
	K_s	0.81	AAT	15.6	5.4	11.08 ± 0.01	11.18 ± 0.01	11.82 ± 0.01	17.76
		$\cdots$	2MASS	13.9	6.0	11.31 ± 0.08	11.45 ± 0.08	12.15 ± 0.03	17.06
		$\cdots$	DENIS	$\cdots$	$\cdots$	11.41 ± 0.06	$\cdots$	$\cdots$	$\cdots$
2MASX J08370723–4339137	J	1.95	2MASS	$\cdots$	2.5	15.92 ± 0.37	$\cdots$	16.33 ± 0.40	19.91
	H	1.24	2MASS	$\cdots$	2.2	14.55 ± 0.25	$\cdots$	14.62 ± 0.19	18.24
	K_s	0.79	AAT	7.3	2.7	13.13 ± 0.01	13.24 ± 0.01	13.29 ± 0.01	17.50
		$\cdots$	2MASS	5.4	3.0	13.51 ± 0.22	13.71 ± 0.14	13.77 ± 0.14	17.89

Table columns: (1) Source name; (2) NIR band; (3) extinction within the given band; (4) telescope; (5) r_{20} is the radius at 20 mag arcsec^{-2}; (6) r_{eff} is the integrated half-light radius; (7) m_{tot} is the total apparent magnitude; (8) m_{20} is the 20 mag arcsec^{-2} elliptical isophotal magnitude (9) $m(r<5'')$ is the $5''$ circular aperture magnitude; and (10) $SB(r_{eff})$ is the mean surface brightness at r_{eff}.

Table 5. NIR colours corrected for galactic foreground extinction

Colour	HIZOA J0836–43			2MASX J08363600–4337556			2MASX J08370723–4339137
	AAT	2MASS	DENIS	AAT	2MASS	DENIS	2MASS
$(I-J)^o_T$	$\cdots$	$\cdots$	1.07	$\cdots$	$\cdots$	1.13	$\cdots$
$(I-J)^o_{7''}$	$\cdots$	$\cdots$	0.64	$\cdots$	$\cdots$	0.76	$\cdots$
	$\cdots$	$\cdots$	$\cdots$	$\cdots$	$\cdots$	$\cdots$	$\cdots$
$(I-K_s)^o_T$	$\cdots$	$\cdots$	2.00	$\cdots$	$\cdots$	2.17	$\cdots$
$(I-K_s)^o_{7''}$	$\cdots$	$\cdots$	1.50	$\cdots$	$\cdots$	1.49	$\cdots$
	$\cdots$	$\cdots$	$\cdots$	$\cdots$	$\cdots$	$\cdots$	$\cdots$
$(J-K_s)^o_T$	$\cdots$	1.10	0.93	$\cdots$	0.88	1.04	1.25
$(J-K_s)^o_{5''}$	$\cdots$	0.93	0.87*	$\cdots$	0.77	0.72*	1.40
	$\cdots$	$\cdots$	$\cdots$	$\cdots$	$\cdots$	$\cdots$	$\cdots$
$(H-K_s)^o_T$	0.43	0.12	$\cdots$	0.46	0.07	$\cdots$	0.59
$(H-K_s)^o_{5''}$	0.39	0.23	$\cdots$	0.34	0.15	$\cdots$	0.40
	$\cdots$	$\cdots$	$\cdots$	$\cdots$	$\cdots$	$\cdots$	$\cdots$
$(J-H)^o_T$	$\cdots$	0.98	$\cdots$	$\cdots$	0.81	$\cdots$	0.66
$(J-H)^o_{5''}$	$\cdots$	0.70	$\cdots$	$\cdots$	0.62	$\cdots$	1.00

Note: *measured at $7''$.

Table 6. NIR Tully-Fisher comparisons

Mag	Intercept[a]	Slope[a]	M_λ(TF)	M_λ(phot)	Δ(TF-phot)
I_T	-21.10	-8.7	-23.88	-23.92 (DE)	$+0.04$ (DE)
H_T	-22.40	-10.0	-25.60	-25.52 (AAT)	-0.08 (AAT)
				-25.81 (2M)	$+0.21$ (2M)
K_T	-22.66	-9.9	-25.82	-26.04 (AAT)	$+0.22$ (AAT)
				-25.90 (2M)	$+0.08$ (2M)
				-25.72 (DE)	-0.10 (DE)
H_{20}	-22.01	-10.5	-25.37	-25.41 (AAT)	$+0.04$ (AAT)
				-25.44 (2M)	$+0.07$ (2M)
K_{20}	-22.34	-10.4	-25.67	-25.84 (AAT)	$+0.17$ (AAT)
				-25.56 (2M)	-0.11 (2M)

Notes: (a) Intercept and slope were taken from Macri 2001.

Table 7. H I measurements and derived properties of some of the most H I-massive galaxies known.

H I source	$v_{\rm hel}$ [km s^{-1}]	D [Mpc]	$F_{\rm HI}$ Jy km s^{-1}	$\log M_{\rm HI}$ [$M_\odot$]	w_{50}	w_{20}	Ref., comments
UGC 4288	30223	433	2.54	11.05	520	558	1, Arecibo
UGC 1752	17861	249	5.13	10.87	388	429	2, Nancay
HIZOA J0836–43	10689	148	14.5	10.87	566	610	3, ATCA image
Malin 1	24784	351	1.8	10.72	293	341	2, Nancay
”	24755	”	2.5	10.86		322	4, VLA image
”	24705	”	2.7	10.89	295	355	5, Arecibo
”	24745	”	4.6	11.13	315	340	6, NRAO 43-m

References: (1) O'Neil et al. 2004, (2) Matthews et al. 2001, (3) this paper, (4) Pickering et al. 1997, (5) Bothun et al. 1987, and (6) Impey & Bothun 1989. **Notes:** The heliocentric velocity, $v_{\rm hel}$, given in Col.(2), was used to calculate the luminosity distance, D, given in Col.(3) as described in Section 4.